Acetylene-mediated Electron Transport in Nanostructured Graphene and Hexagonal Boron Nitride

Isaac Alcón[1,2]*, Nick Papior[3], Gaetano Calogero[4], Francesc Viñes[5]*, Pablo Gamallo[5] and Mads Brandbyge[6,7]

[1]*Catalan Institute of Nanoscience and Nanotechnology (ICN2), Av. de Serragalliners, s/n, 08193 Bellaterra (Barcelona), Spain*

[2]*Institut für Chemie und Biochemie, Physikalische und Theoretische Chemie, Freie Universität Berlin, Arnimallee 22, 14195 Berlin, Germany*

[3]*Computing Center, Technical University of Denmark, DK-2800 Kongens Lyngby, Denmark*

[4]*CNR Institute for Microelectronics and Microsystems (CNR-IMM), Strada VIII, 5, 95121 Catania, Italy*

[5]*Departament de Ciència de Materials i Química Física & Institut de Química Teòrica i Computacional (IQTCUB), Universitat de Barcelona, c/ Martí i Franquès 1-11, 08028 Barcelona, Spain*

[6]*Department of Physics, Technical University of Denmark, DK-2800 Kongens Lyngby, Denmark*

[7]*Center for Nanostructured Graphene (CNG), DK-2800 Kongens Lyngby, Denmark*

*Corresponding authors: isaac.alcon@icn2.cat, francesc.vines@ub.edu

Abstract

The discovery of graphene has catalysed the search for other 2D carbon allotropes, such as graphynes, graphdiynes, and 2D π-conjugated polymers, which have been theoretically predicted or experimentally synthesized during the last decade. These materials exhibit a conductive nature bound to their π-conjugated sp^2 electronic system. Some cases include *sp*-hybridized moieties in their nanostructure, such as acetylenes in graphynes, however, these merely act as electronic couplers between the conducting π-orbitals of sp^2 centres. Here, *via* first principles calculations and quantum transport simulations, we demonstrate the existence of an acetylene-meditated transport mechanism entirely hosted by *sp*-hybridized orbitals. For that we propose a series of nanostructured 2D materials featuring linear arrangements of closely packed acetylene units which function as *sp*-nanowires. Due to the very distinct nature of this unique transport mechanism, it appears to be highly complementary with π-conjugation, thus potentially becoming a key tool for future carbon nanoelectronics.

TOC Graphic

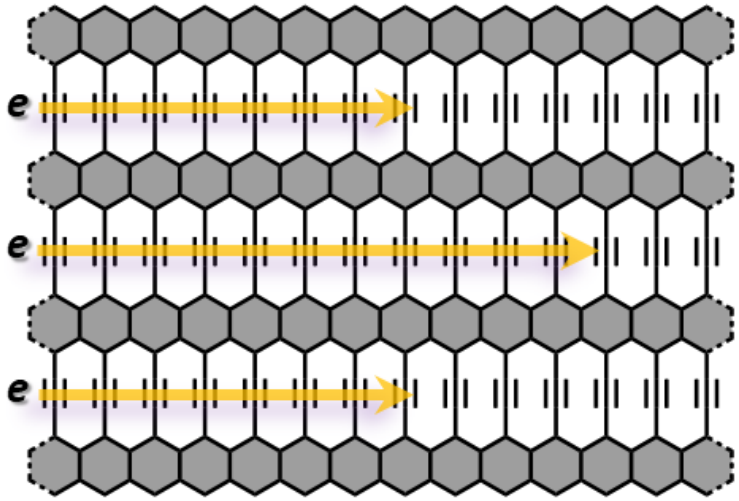

Carbon atoms with sp^2 orbital hybridization are the basic building block of various carbon allotropes that have revolutionized materials science in the last few decades,[1,2] starting from fullerenes discovery,[3] continuing with carbon nanotubes,[4] and, more recently, graphene.[5] The two-dimensional (2D) form of sp^2 carbon, graphene, has led to the whole new area of 2D materials,[6–8] and their van der Waals heterostructures,[9] and it has been the platform gathering the most important world-wide efforts towards carbon-based nanoelectronics.[10–12] The existence of linearly dispersing bands crossing at the Fermi level, *i.e.* a Dirac cone, in graphene has generated great enthusiasm in condensed-matter physics. This feature arises from its π-conjugated electronic structure and has launched a global search for other π-conjugated 2D carbon allotropes which may host this unique characteristic. In this line, different types of the so-called post-graphene organic Dirac materials (or PGODs) have been theoretically predicted, with the most notable examples being graphynes,[13–15] graphdiynes,[16–19] and 2D π-conjugated organic polymers.[20–24] Importantly, different members of PGODs have been recently synthesized.[17,25–28]

In all these materials charge transport takes place in the π-conjugated system, and so *via* sp^2 carbon atoms. This is also true for the sp/sp^2 hybridized graphynes and graphdiynes, where sp^2 carbon centers are connected *via sp* acetylenic units, also regarded as C_{sp}-C_{sp} triple bonds. In such materials the transport mechanism is still π-conjugated in nature, and so replacing acetylene units by other conjugated functional groups such as benzene, thiophene or ethylene gives rise to qualitatively the same electronic structure (*e.g.* Dirac cones).[20,21]

Here, employing first principles calculations and large-scale transport simulations, we demonstrate the existence of unconventional *sp*-hybridized charge transport in a new type of nanostructured 2D materials. We propose 2D covalent arrays of graphene or hexagonal boron-nitride (*h*-BN) nanoribbons laterally connected *via* acetylene units. The unique nanostructure of such materials displays acetylene units in very close proximity to each other in a linear, ordered fashion, which leads to the appearance of strongly dispersive *sp*-hybridized bands near the Fermi level. Our simulations demonstrate these bands give rise to a new charge transport mechanism exclusively involving the densely packed acetylene rows. As a result, the π-conjugated graphene or *h*-BN nanoribbons simply act as coupling media between neighboring *sp*-wires, and so the wider the nanoribbons the less electronically coupled the *sp*-wires and, consequently, the more collimated their wavefunction. This close arrangement of acetylene units is not possible in hexagonal carbon frameworks, such as graphynes, graphdiynes, or π-conjugated 2D polymers, which explains why such a simple, yet effective, transport mechanism has not been reported previously, in spite of the great number of carbon nanostructured materials investigated in the last years. Given the inherently distinct nature of such electronic *sp*-hybridized transport, we forecast it may well be potentially used in the future as a complementary tool to π-conjugation. For instance, here we demonstrate it may be utilized to provide conducting characteristics to *h*-BN nanostructures, which are otherwise electrically insulating systems.[29]

The optimized atomic structures of the considered acetylene graphene (AcGr_i) and acetylene hexagonal boron-nitride (AcBN_i) nanostructures are shown in Fig. 1, where the index (*i*=1-3) indicates the width of the graphene or *h*-BN nanoribbons. All materials have been optimized using the PBE functional in periodic DFT calculations, where both atomic positions and unit cell parameters have been fully relaxed (see Methods section for details). Previous work on AcGrs (therein referred as grazynes) demonstrated these are fully planar 2D nanostructured materials.[30] AcGrs and AcBNs nanostructures can be regarded as 2D parallel arrays of zig-zag graphene or *h*-BN nanoribbons, covalently connected *via* acetylene units, thus displaying a similarity with the recently bottom-up synthesized nanoporous graphene.[31]

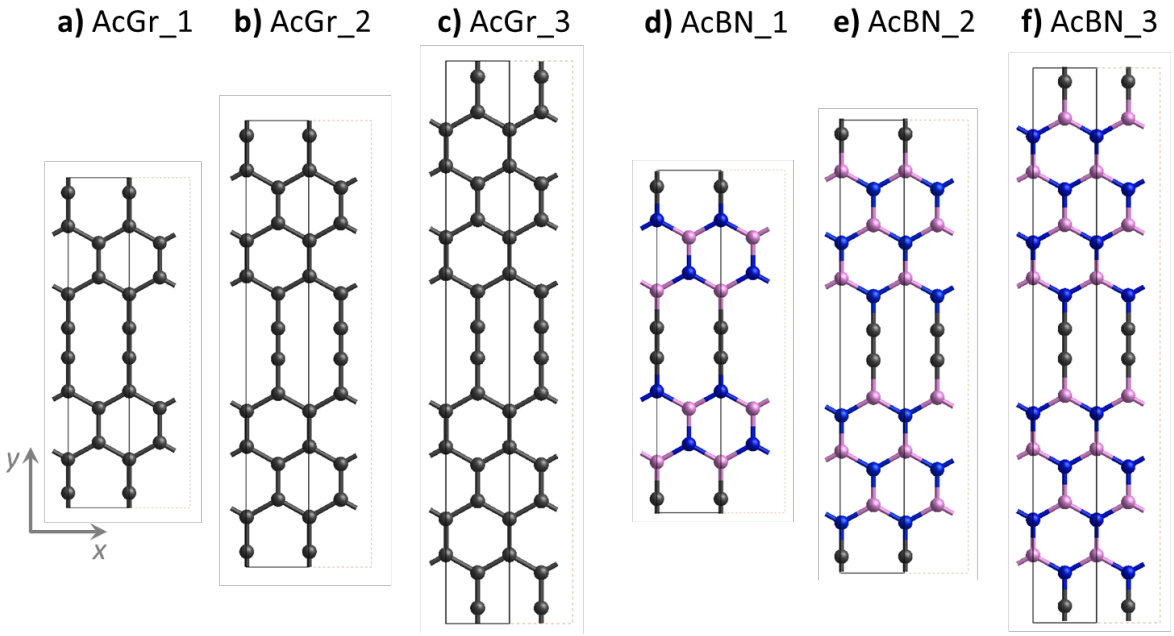

Fig. 1. Atomic structure of a) AcGr_1, b) AcGr_2, c) AcGr_3, d) AcBN_1, e) AcBN_2, and f) AcBN_3, where the utilized unit cell is highlighted. Atom coloring: C – grey, B – purple, N – blue.

In Fig. 2a,b we plot the orbital-resolved band structures for AcGr_1 and AcBN_1, respectively, where one may see that the low-energy spectra for both types of materials is mainly composed by p_z and p_xp_y bands, shown in green and blue, respectively. Note that p_z bands are associated with the sp^2 π-conjugated system (*i.e.* the nanoribbons), whereas the p_xp_y bands arise from *sp* centers, *i.e.* the acetylene units. The electronic structure for the remaining members of each family of materials is qualitatively similar, as shown in Fig. S1 and S2 of the Supporting Information (SI). The main difference between AcGrs and AcBNs is the presence of a π-conjugated Dirac cone in the former (Fig. 2a). We note that such Dirac cone in AcGrs is slightly electron doped, pinning the p_xp_y bands at the Fermi energy, E_F. This arises from the well-known over-delocalization of generalized gradient approximation (GGA) functionals, such as the here employed PBE.[21] However, the qualitative features of our reported band structures match those obtained in previous studies using hybrid functionals,[30] where this over-delocalization is counteracted. The parabolic p_xp_y bands appear in the valence band for both types of materials (Fig. 2a,b) being pinned at E_F for AcGrs, and appearing lower in energy for AcBNs, which display a finite bandgap.

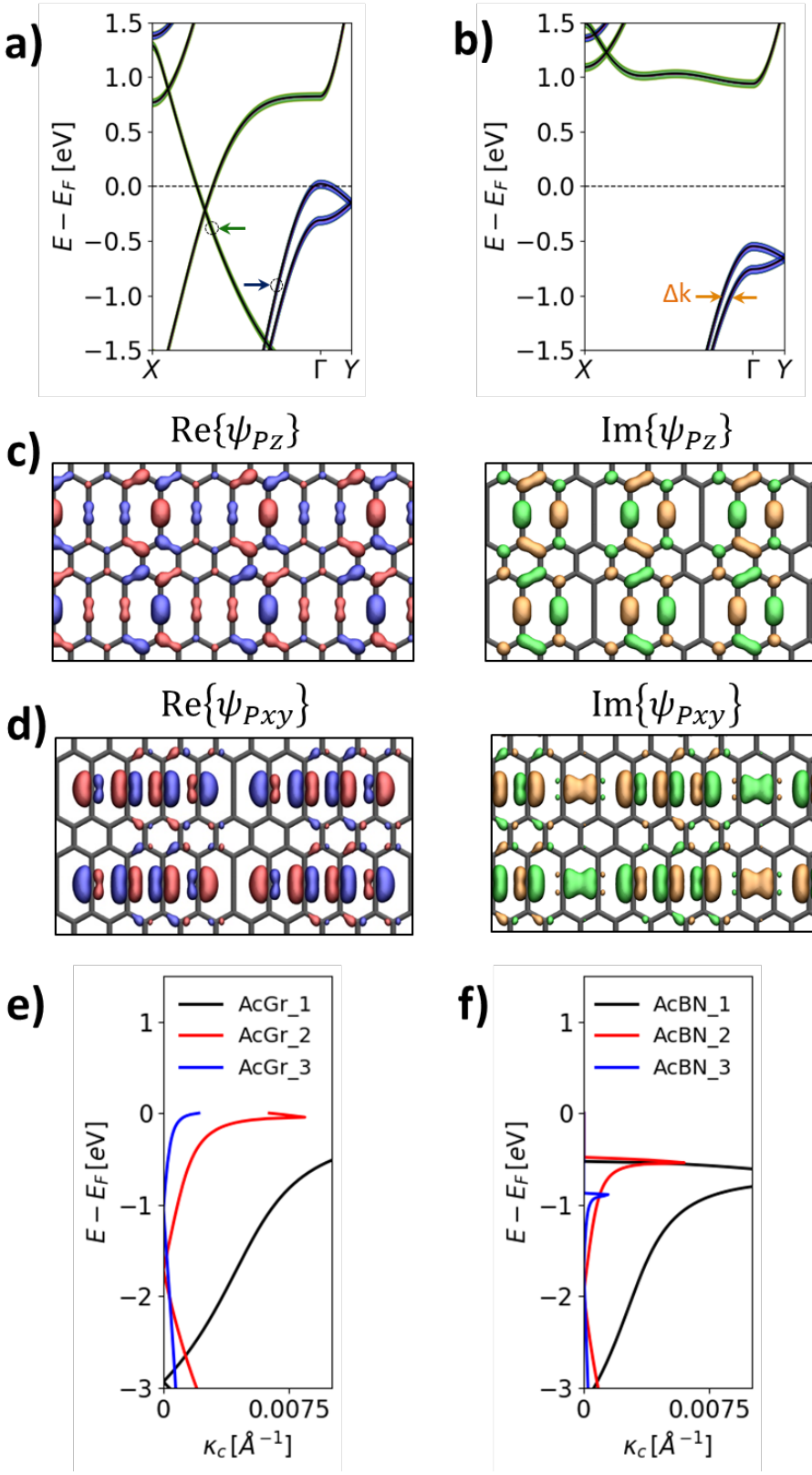

Fig. 2. Orbital-resolved band structure for a) AcGr_1 and b) AcBN_1, where p_z and p_xp_y bands are coloured in green and blue, respectively. Δk is extracted between the two p_xp_y longitudinal bands along the Γ→X path, as indicated with the orange arrows in b. c), d) Spatial projections of the real (Re, left) and imaginary (Im, right) parts of the p_z (k_x = 1/3) and p_xp_y (k_x = 1/10) wavefunctions, respectively, in AcGr_1 along the Γ→X path (see arrows indicating specific locations in a). e), f) κ_c spectra calculated as $\kappa_c = \Delta k/4$ for the p_xp_y bands in AcGrs and AcBNs, respectively.

In Fig. 2c,d we show the spatial projection of the real (left panels) and imaginary (right panels) parts of the p_z and $p_x p_y$ wavefunctions, respectively, for the AcGr_1 along the $\Gamma \rightarrow X$ segment (see arrows in Fig. 2a for specific energies). Taking a look at ψ_{Pz} (Fig. 2c) one may see that it is fully spread over the entire atomic structure. This is in agreement with the fully delocalized nature of linear dispersive bands crossing at E_F, *i.e.* Dirac cones (Fig. 2a). ψ_{PxPy} displays a very different behaviour (Fig. 2d). On the one hand, ψ_{PxPy} is composed of $pp\sigma$ type interactions between adjacent acetylene units, with characteristic nodes in the *yz* plane at each acetylene unit. On the other hand, and contrary to that observed for ψ_{Pz} (Fig. 2c), ψ_{PxPy} is strongly localized on the acetylenic rows (Fig. 2d), with a very minor contribution in the graphene nanoribbons. We note ψ_{PxPy} shows a very similar spatial distribution for AcBN_1 (see Fig. S3 in the SI). The spatially linear dispersion of ψ_{PxPy} for both AcGr_1 and AcBN_1 clearly suggests the existence of an unconventional $pp\sigma$ type transport mechanism taking place exclusively between adjacent acetylene units which, consequently, should exhibit a significant anisotropic character.

In order to assess such a possibility we constructed large-scale devices based on DFT-parametrized TB models for each considered material (see the Methods section for details). Such devices allow for injecting currents in specific atomic locations, thus mimicking charge injection *via* a scanning tunnelling microscope (STM) tip.[32] In order to explore the acetylene-mediated transport mechanism we have to inject currents in the occupied region of the band structure, where the $p_x p_y$ bands are located (see Fig. 2a,b). This could be experimentally achieved by applying positive STM tip bias to probe occupied sample states, doping the system[33,34] or applying electrostatic gates, as regularly done for graphene.[35,36] In Fig. 3 we show the bond current maps upon injecting at $E–E_F$ = -0.5 eV on the left side of large-scale devices made of AcGr_1, AcGr_2, and AcGr_3. These devices have been constructed by repeating each unit cell, shown in Fig. 1, a number of times along *x* and *y* directions (see Methods section for details) and are composed of 51744, 53312, and 55440 atoms, respectively. In the left panels of Fig. 3 we show the zoomed bond currents around the point of injection (source; red dot) for each device. There one may clearly see for all cases that electron transport takes place primarily through a hopping mechanism between adjacent acetylene units, with an almost negligible bond current density in the graphene nanoribbons. Such transport mechanism also takes place in the analogous AcBNs (see associated bond-currents at $E-E_F$ = -1.0 eV in Fig. S4 of the SI) where there exists a slight, yet minor, increase of bond current spreading through the nitrogen connections of the BN nanoribbons. As far as we know, in spite of the great number of acetylene-containing carbon 2D materials previously reported, both theoretically[13–16] and experimentally,[27,28] this is hitherto the first reported instance of $pp\sigma$ acetylene-mediated electron transport.

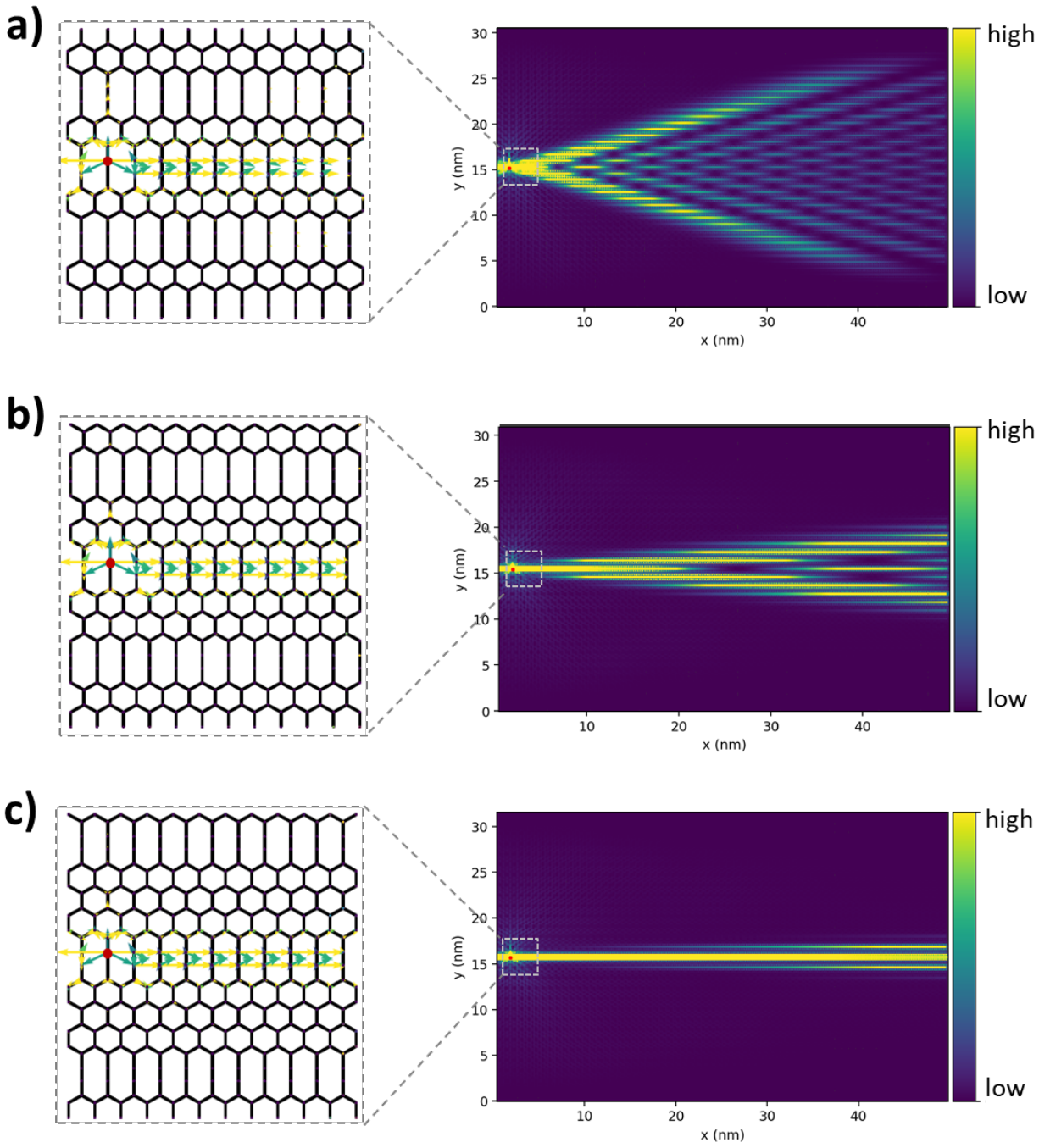

Fig. 3. Bond current maps of injected currents in large-scale devices made of a) AcGr_1 (51,744 atoms), b) AcGr_2 (53,312 atoms) and c) AcGr_3 (55,440 atoms) at $E–E_F$ = -0.5 eV. Left panels provide a zoomed view in an area around the injection point (*ca.* 3.0 x 3.0 nm^2). Small red dots on the left region of devices indicate the point of current injection. Regions with high current density are shown in bright yellow and those with low or no current density are shown in dark purple, as indicated with color bars.

The large-scale devices bond currents shown in the right panels in Fig. 3 reveal a Talbot interference pattern of injected currents far from the source, which is a typical feature of optical waveguides,[37,38] but has also been recently reported for weakly electronically coupled GNR arrays (known as nanoporous graphenes).[32,39] To obtain such an effect the injection energy needs to cross both p_xp_y longitudinal bands because, in case of crossing a single state

(as it may happen very close to E_F), no interference pattern occurs (see Fig. S5 in the SI). The degree of electronic coupling between the two 1D nanoelectronic channels (in our case the acetylene wires) is well captured by the inter-channel coupling coefficient, κ_c. This energy-dependent parameter is extracted from the band structure of each 2D material as the momentum difference between the relevant longitudinal bands, as $\kappa_c = \Delta k/4$ [32] — see Δk in Fig. 2b. In Fig. 2e we provide the κ_c spectra for AcGr_1, AcGr_2, and AcGr_3, showing a significant difference along the materials series. Particularly, at $E–E_F$ = -0.5 eV the κ_c value for AcGr_1 is much larger than those for AcGr_2, and AcGr_3, being almost negligible for the latter. Similar κ_c results are obtained for AcBNs, but at lower energies (see Fig. 2f). As we may see in the right panels of Fig. 3, such a tendency in κ_c is clearly reflected in the resulting spreading of currents injected on the different AcGrs at $E–E_F$ = -0.5 eV. Within AcGr_1, with the highest electronic coupling, currents quickly spread through a number of acetylenic wires, being distributed throughout the entire width of the device when reaching the right electrode, see Fig. 3a. This changes significantly for both AcGr_2 and AcGr_3, which, in accordance with their respective κ_c spectra (Fig. 2e), show a much reduced spreading of currents along the *y*-direction as they propagate towards the right electrode. Such collimation effect is particularly significant for AcGr_3, where currents stay confined in the single acetylene-wire they were injected for almost 30 nm from the source, showing only a minor spreading to its first neighbouring channels at the right end of the device, see Fig. 3c. This trend, reminiscent of previously studied GNR arrays,[39] highlights the electronic decoupling role of the π-conjugated GNRs, so that the wider these are, the less electronically coupled the acetylene-wires become, see *e.g.* AcGr_3 in Fig. 3c. Such overall behaviour with increasing nanoribbon thickness is also observed for the analogous AcBN series, as shown in Fig. S4. We note that injecting on a GNR atomic position partially increases the π-conjugated isotropic current spreading around the injection point (see Fig. S6a in the SI). Such an effect is not observed in the analogous AcBN material (see Fig. S6b in the SI), due to the lack of available states arising from hBN nanoribbons.

The acetylene mediated transport mechanism herein reported arises from the specific geometry of AcGrs and AcBNs, which keeps the periodically arranged acetylene units in close proximity, enabling an effective p_xp_y orbital overlap. This can be demonstrated by designing an AcGr_1 where every second acetylene unit is removed, see Fig. 4a (herein labelled *x*-alternating AcGr_1, or *x*-alt-AcGr_1).[30] As it may be seen in Fig. 4b, the resulting electronic band structure is now purely of π-conjugated nature, with the presence of a Dirac cone, but now lacking any p_xp_y bands near the E_F. Consequently, upon injecting currents at $E–E_F$ = -0.5 eV one obtains the well-known six-fold spreading of currents (Fig. 4c) typical for Dirac materials, like graphene.[40,41] This further demonstrates that the p_xp_y nanoelectronic channels, giving rise to the Talbot interference pattern shown in Fig. 3, arise from the close packing of acetylene units in AcGrs and AcBNs generated by their connection through the zig-zag termination of nanoribbons. Note that such dense packing is not possible with other terminations, such as in arm-chair nanoribbons.[42]

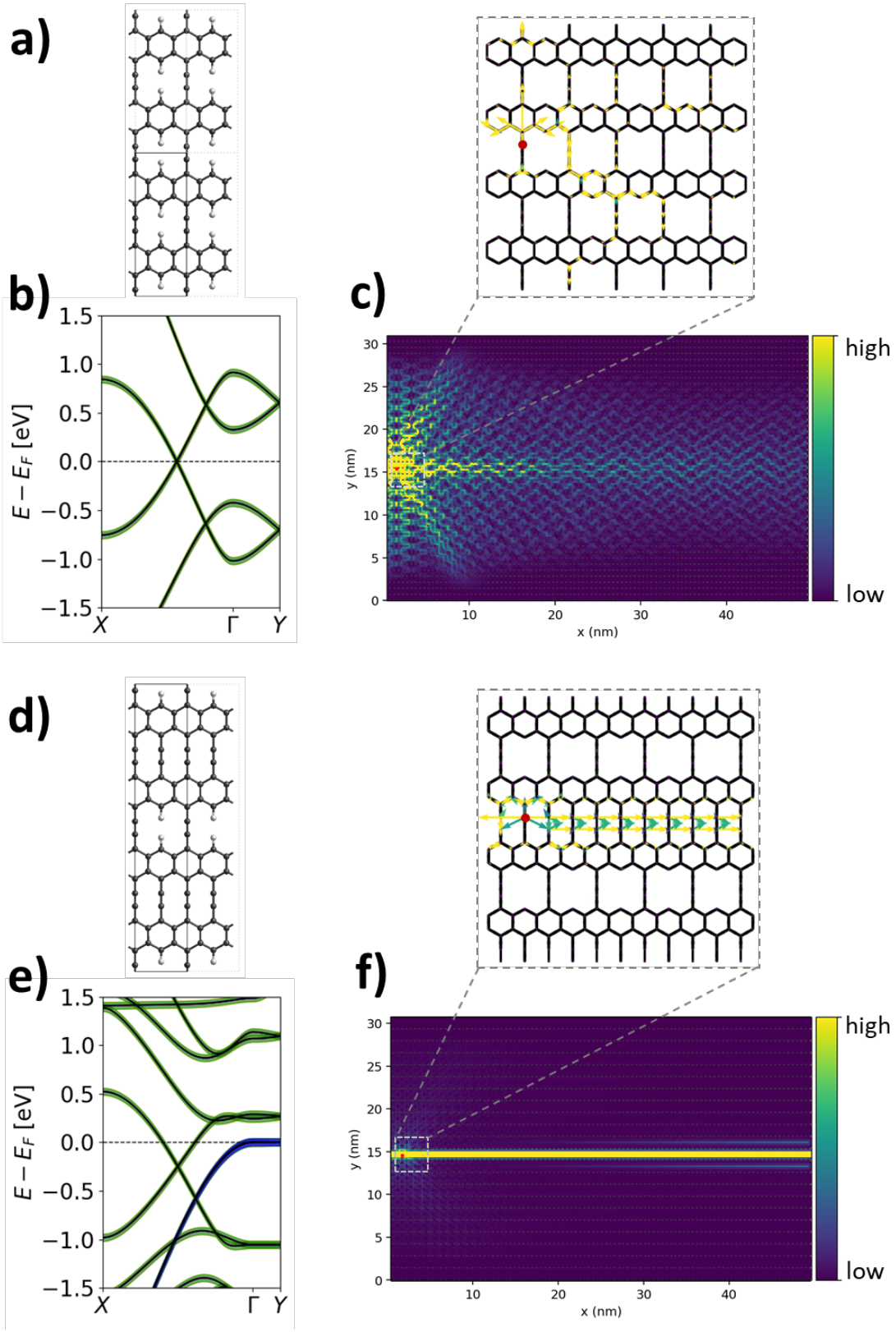

Fig. 4. Atomic periodic unit cells (a, d) and orbital-resolved electronic band structures (b, e) for *x*-alt-AcGr_1 and *xy*-alt-AcGr_1, respectively. p_z fat bands appear in green, and p_xp_y in blue. Bond current maps of injected currents in large-scale devices made of c) *x*-alt-AcGr_1 and f) *xy*-alt-AcGr_1 at $E–E_F$ = -0.5 eV. Top panels provide a zoomed view in an area around the injection point (*ca.* 3.0 x 3.0 nm^2). Small red dots at the left region of the devices indicate the point of current injection. Regions with high

current density are shown in bright yellow and those with low or no current density are shown in dark purple, as indicated with color bars.

Finally, In Fig. 4d we propose the *xy*-alt-AcGr_1, where the alternant acetylene removal has only been done within every second acetylene wire. As it may be observed in Fig. 4e, this brings back the p_xp_y bands close to the E_F, however, due to the larger distance between acetylene wires, these are strongly decoupled, as shown with the associated κ_c spectra in Fig. S7. As a result, injected electrons are strongly collimated on a single acetylene channel for up to 50 nm from the injection point (Fig. 4f), as opposed to the parent AcGr_1, where currents are fully spread throughout the entire device at such distances (Fig. 3a).

Summing up, in this work we propose AcGrs and AcBNs as nanomaterials hosting, to the best of our knowledge, the first instance of $pp\sigma$ acetylene-mediated electronic transport. Such novel transport mechanism is independent on the π-conjugated system, which explains the very similar current characteristics upon using either semimetallic GNRs or insulating BN nanoribbons as π-conjugated coupling elements between the acetylenic wires. The p_xp_y bands appear very close to E_F, which suggests these electronic channels should be readily accessible *via* moderate electrode bias, doping, or electrostatic gates. The existence of such p_xp_y bands in AcGrs is, in fact, the main difference between this family of materials and the well-known *sp*-sp^2 hybridized graphynes[13–15] and graphdiynes,[16–19] which also display a π-conjugated Dirac cone in their electronic band structure. Bond current analysis of the quantum transport simulations demonstrate that our reported transport mechanism uniquely arises from the interaction between closely packed adjacent acetylene units, which is only possible when acetylenes are connected via zig-zag edged, either graphene or BN, nanoribbons. The electronic coupling between acetylene nanowires strongly decreases by increasing the nanoribbon width, with very minor differences between the two types of ribbons. This allows designing 2D arrays of nearly electronically isolated acetylene wires, which is even more pronounced upon alternating such nanowires within the 2D materials, as in *xy*-alt-AcGr_1.

Therefore, our results provide a simple recipe to integrate an unconventional charge transport mechanism in carbon and BN nanostructures. To the best of our knowledge, such phenomenon has not been previously reported before neither experimentally nor *via* computational modelling. Due to its very distinct nature as compared to the standard π-conjugated transport, acetylene-mediated conduction may be highly complementary to the former. As a first example in this regard, here we demonstrated it may provide BN nanostructures with (semi) conducting properties which, otherwise, when purely made of sp^2 centers, behave as electrical insulators.[29]

Computational Methods

The reported graphene and *h*-BN nanostructures have been modelled with density functional theory (DFT) calculations using the Perdew-Burke-Ernzerhof (PBE)[43] exchange correlation functional, a single-ζ basis set with 0.02 Ry energy shift, norm-conserving Troullier−Martins pseudopotentials, and a real-space mesh cut-off of 400 Ry. Monkhorst−Pack **k**-point meshes of 200×65×1, 200×52×1 and 200×45×1 were utilized for the AcGr_1 (AcBN_1), AcGr_2 (AcBN_2),

and AcGr_3 (AcBN_3) nanomaterials, respectively, and 100×65×1 and 100×50×1 for the *x*-alt-AcGr_1 and *xy*-alt-AcGr_1, respectively (see below for structural details). Atomic coordinates and in-plane unit cell vectors were optimized until all forces were below 0.02 eV/Å. The planarity of this type of nanostructures was previously reported,[30] and so all materials were optimized from fully flat geometries. Large-scale quantum transport was modelled by extracting the on-site and coupling elements of *s*, p_x, p_y and p_z orbitals from the DFT Hamiltonian to parametrize an efficient tight-binding (TB) model capturing the low-energy spectra — see DFT benchmark in Fig. S8 of the SI. This procedure was done using the open-source Python-based SISL utility.[44] The large-scale TB models were constructed by repeating the primitive unit cell (utilized for DFT calculations) along x and y directions until reaching approximately 50 x 30 nm^2 device sizes, leading to samples composed of over 45,000 atoms. These large structures are fed to the open-source TBtrans code[45] to simulate quantum transport using the Green's function formalism.[46–48] Periodic boundary conditions are not utilized in these large-scale simulations. Current injection is modelled *via* a constant, on-site level broadening $i\Gamma$ self-energy in the device Green's function,[49] located on a single atom (see red dot in each device). Currents are drained along the *x* direction (longitudinal to *sp*-channels) into two semi-infinite AcGr-like (or AcBN-like) electrodes placed at the two terminations of the device along *x*, and absorbed by 5 nm wide regions at the bottom and top extremes equipped with complex absorbing potentials (CAP).[50,51] More information on this type of large-scale transport simulations is described in detail elsewhere.[32,39,41] The spatial distribution of current flow is represented via plotting 2D bond-current maps, scaling the colour-map in proportion to the current magnitude flowing out of each atom, so that areas with low to zero current appear dark.

Conflicts of interest

No conflicts of interest to declare.

Acknowledgements

I.A. is grateful for a Humboldt postdoctoral fellowship from the Alexander von Humboldt Foundation and a *Juan de la Cierva* postdoctoral grant (FJC2019-038971-I) from the *Ministerio de Ciencia e Investigación*. Financial support by Villum Fonden (00013340) is gratefully acknowledged. ICN2 is funded by the CERCA Programme from *Generalitat de Catalunya* and is supported by the Severo Ochoa program from Spanish MINECO (Grant No. SEV-2017-0706). The Center for Nanostructured Graphene (CNG) is sponsored by the Danish National Research Foundation (DNRF103). This work has also been supported by the Spanish MICIUN/FEDER RTI2018-095460-B-I00, RTI2018-094757-B-I00, and *María de Maeztu* MDM-2017-0767 grants and, in part, by *Generalitat de Catalunya* 2017SGR13 grant.

Supporting Information

Supporting Information Available: Benchmarking of parametrized TB models; orbital resolved band structures for AcGrs; orbital resolved band structures for AcBNs; spatial projection of the p_xp_y wavefunction in AcBN_1; bond currents in AcBNs large-scale devices; k_c spectra for AcGr_1 and *xy*-alt-AcGr_1.

References

(1) Hirsch, A. The Era of Carbon Allotropes. *Nat. Mater.* **2010**, *9* (11), 868–871.

(2) Diederich, F.; Rubin, Y. Synthetic Approaches toward Molecular and Polymeric Carbon Allotropes. *Angew. Chemie Int. Ed. English* **1992**, *31* (9), 1101–1123.

(3) Kroto, H. W.; Heath, J. R.; O'Brien, S. C.; Curl, R. F.; Smalley, R. E. C60: Buckminsterfullerene. *Nature* **1985**, *318* (6042), 162–163.

(4) Iijima, S. Helical Microtubules of Graphitic Carbon. *Nature* **1991**, *354*, 56–58.

(5) Novoselov, K. S.; Geim, A. K.; Morozov, S. V.; Jiang, D.; Zhang, Y.; Dubonos, S. V.; Grigorieva, I. V.; Firsov, A. A. Electric Field Effect in Atomically Thin Carbon Films. *Science (80-.).* **2004**, *306* (5696), 666–669.

(6) Nicolosi, V.; Chhowalla, M.; Kanatzidis, M. G.; Strano, M. S.; Coleman, J. N. Liquid Exfoliation of Layered Materials. *Science (80-.).* **2013**, *340* (6139), 1226419–1226419.

(7) Das, S.; Robinson, J. A.; Dubey, M.; Terrones, H.; Terrones, M. Beyond Graphene: Progress in Novel Two-Dimensional Materials and van Der Waals Solids. *Annu. Rev. Mater. Res.* **2015**, *45* (1), 1–27.

(8) Liu, X. H.; Guan, C. Z.; Wang, D.; Wan, L. J. Graphene-like Single-Layered Covalent Organic Frameworks: Synthesis Strategies and Application Prospects. *Adv. Mater.* **2014**, *26* (40), 6912–6920.

(9) Britnell, L.; Gorbachev, R. V.; Jalil, R.; Belle, B. D.; Schedin, F.; Mishchenko, A.; Georgiou, T.; Katsnelson, M. I.; Eaves, L.; Morozov, S. V.; et al. Field-Effect Tunneling Transistor Based on Vertical Graphene Heterostructures. *Science (80-.).* **2011**, *335*, 947–950.

(10) Geim, A. K.; Novoselov, K. S. The Rise of Graphene. *Nat. Mater.* **2007**, *6* (3), 183–191.

(11) Schwierz, F. Graphene Transistors. *Nat. Nanotechnol.* **2010**, *5* (7), 487–496.

(12) Schwierz, F. Graphene Transistors: Status, Prospects, and Problems. *Proc. IEEE* **2013**, *101* (7), 1567–1584.

(13) Malko, D.; Neiss, C.; Viñes, F.; Görling, A. Competition for Graphene: Graphynes with Direction-Dependent Dirac Cones. *Phys. Rev. Lett.* **2012**, *108* (8), 086804.

(14) Chen, J.; Xi, J.; Wang, D.; Shuai, Z. Carrier Mobility in Graphyne Should Be Even Larger than That in Graphene: A Theoretical Prediction. *J. Phys. Chem. Lett.* **2013**, *4* (9), 1443–1448.

(15) Kim, B. G.; Choi, H. J. Graphyne: Hexagonal Network of Carbon with Versatile Dirac Cones. *Phys. Rev. B* **2012**, *86* (11), 115435.

(16) Xi, J.; Wang, D.; Shuai, Z. Electronic Properties and Charge Carrier Mobilities of Graphynes and Graphdiynes from First Principles. *Wiley Interdiscip. Rev. Comput. Mol. Sci.* **2015**, *5* (2), 215–227.

(17) Li, Y.; Xu, L.; Liu, H.; Li, Y. Graphdiyne and Graphyne: From Theoretical Predictions to Practical Construction. *Chem. Soc. Rev.* **2014**, *43* (8), 2572–2586.

(18) Serafini, P.; Milani, A.; Proserpio, D. M.; Casari, C. S. Designing All Graphdiyne Materials

as Graphene Derivatives: Topologically Driven Modulation of Electronic Properties. *J. Phys. Chem. C* **2021**, *125* (33), 18456–18466.

(19) Serafini, P.; Milani, A.; Tommasini, M.; Bottani, C. E.; Casari, C. S. Topology-Dependent Conjugation Effects in Graphdiyne Molecular Fragments. *Carbon N. Y.* **2021**, *180*, 265–273.

(20) Adjizian, J.-J.; Briddon, P.; Humbert, B.; Duvail, J.-L.; Wagner, P.; Adda, C.; Ewels, C. Dirac Cones in Two-Dimensional Conjugated Polymer Networks. *Nat. Commun.* **2014**, *5*, 5842.

(21) Alcón, I.; Viñes, F.; Moreira, I. de P. R.; Bromley, S. T. Existence of Multi-Radical and Closed-Shell Semiconducting States in Post-Graphene Organic Dirac Materials. *Nat. Commun.* **2017**, *8* (1), 1957.

(22) Thomas, S.; Li, H.; Bredas, J.-L. Emergence of an Antiferromagnetic Mott Insulating Phase in Hexagonal π-Conjugated Covalent Organic Frameworks. *Adv. Mater.* **2019**, 1900355.

(23) Jing, Y.; Heine, T. Two-Dimensional Kagome Lattices Made of Hetero Triangulenes Are Dirac Semimetals or Single-Band Semiconductors. *J. Am. Chem. Soc.* **2019**, *141* (2), 743–747.

(24) Santiago, R.; Alcón, I.; Ribas-Arino, J.; Deumal, M.; P. R. Moreira, I.; Bromley, S. T. 2D Hexagonal Covalent Organic Radical Frameworks as Tunable Correlated Electron Systems. *Adv. Funct. Mater.* **2020**, *31*, 2004584.

(25) Yang, Y.; Liu, C.; Xu, X.; Meng, Z.; Tong, W.; Ma, Z.; Zhou, C.; Sun, Y.; Sheng, Z. Antiferromagnetism in Two-Dimensional Polyradical Nanosheets. *Polym. Chem.* **2018**, *9* (46), 5499–5503.

(26) Wu, J.; Wu, S.; Li, M.; Phan, H.; Wang, D.; Herng, T. S.; Ding, J.; Lu, Z. Toward π-Conjugated 2D Covalent Organic Radical Frameworks. *Angew. Chemie Int. Ed.* **2018**, *57* (27), 8007–8011.

(27) Li, Z.; Smeu, M.; Rives, A.; Maraval, V.; Chauvin, R.; Ratner, M. A.; Borguet, E. Towards Graphyne Molecular Electronics. *Nat. Commun.* **2015**, *6*, 6321.

(28) Li, G.; Li, Y.; Liu, H.; Guo, Y.; Li, Y.; Zhu, D. Architecture of Graphdiyne Nanoscale Films. *Chem. Commun.* **2010**, *46* (19), 3256–3258.

(29) Wang, S.; Chen, Q.; Wang, J. Optical Properties of Boron Nitride Nanoribbons: Excitonic Effects. *Appl. Phys. Lett.* **2011**, *99* (6), 063114.

(30) Kamalinahad, S.; Viñes, F.; Gamallo, P. Grazynes: Carbon-Based Two-Dimensional Composites with Anisotropic Properties. *J. Phys. Chem. C* **2019**, *123* (44), 27140–27149.

(31) Moreno, C.; Vilas-Varela, M.; Kretz, B.; Garcia-Lekue, A.; Costache, M. V.; Paradinas, M.; Panighel, M.; Ceballos, G.; Valenzuela, S. O.; Peña, D.; et al. Bottom-up Synthesis of Multifunctional Nanoporous Graphene. *Science (80-.).* **2018**, *360* (6385), 199–203.

(32) Calogero, G.; Papior, N. R.; Kretz, B.; Garcia-Lekue, A.; Frederiksen, T.; Brandbyge, M. Electron Transport in Nanoporous Graphene: Probing the Talbot Effect. *Nano Lett.* **2018**, *19* (1), 576–581.

(33) Friedrich, N.; Brandimarte, P.; Li, J.; Saito, S.; Yamaguchi, S.; Pozo, I.; Penã, D.; Frederiksen, T.; Garcia-Lekue, A.; Sánchez-Portal, D.; et al. Magnetism of Topological Boundary States Induced by Boron Substitution in Graphene Nanoribbons. *Phys. Rev. Lett.* **2020**, *125* (14), 146801.

(34) Kawai, S.; Saito, S.; Osumi, S.; Yamaguchi, S.; Foster, A. S.; Spijker, P.; Meyer, E. Atomically Controlled Substitutional Boron-Doping of Graphene Nanoribbons. *Nat. Commun.* **2015**, *6*, 8098.

(35) Nguyen, P. V.; Teutsch, N. C.; Wilson, N. P.; Kahn, J.; Xia, X.; Graham, A. J.; Kandyba, V.; Giampietri, A.; Barinov, A.; Constantinescu, G. C.; et al. Visualizing Electrostatic Gating Effects in Two-Dimensional Heterostructures. *Nature* **2019**, *572* (7768), 220–223.

(36) Bøggild, P.; Caridad, J. M.; Stampfer, C.; Calogero, G.; Papior, N. R.; Brandbyge, M. A Two-Dimensional Dirac Fermion Microscope. *Nat. Commun.* **2017**, *8*, 15783.

(37) Yariv, A.; Yeh, P. *Optical Waves in Crystals: Propagation and Control of Laser Radiation*; Wiley, 2002.

(38) Pertsch, T.; Zentgraf, T.; Peschel, U.; Bräuer, A.; Lederer, F. Anomalous Refraction and Diffraction in Discrete Optical Systems. *Phys. Rev. Lett.* **2002**, *88* (9), 939011–939014.

(39) Calogero, G.; Alcón, I.; Papior, N.; Jauho, A.-P.; Brandbyge, M. Quantum Interference Engineering of Nanoporous Graphene for Carbon Nanocircuitry. *J. Am. Chem. Soc.* **2019**, *141* (33), 13081–13088.

(40) Márk, G. I.; Vancsó, P.; Hwang, C.; Lambin, P.; Biró, L. P. Anisotropic Dynamics of Charge Carriers in Graphene. *Phys. Rev. B* **2012**, *85* (12), 125443.

(41) Calogero, G.; Papior, N.; Koleini, M.; Larsen, M. H. L.; Brandbyge, M. Multi-Scale Approach to First-Principles Electron Transport beyond 100 Nm. *Nanoscale* **2019**, *11*, 6153–6164.

(42) Cai, J.; Ruffieux, P.; Jaafar, R.; Bieri, M.; Braun, T.; Blankenburg, S.; Muoth, M.; Seitsonen, A. P.; Saleh, M.; Feng, X.; et al. Atomically Precise Bottom-up Fabrication of Graphene Nanoribbons. *Nature* **2010**, *466* (7305), 470–473.

(43) Perdew, J. P.; Burke, K.; Ernzerhof, M. Generalized Gradient Approximation Made Simple. *Phys. Rev. Lett.* **1996**, *77* (18), 3865–3868.

(44) Papior, N. Sisl. 2021, p https://github.com/zerothi/sisl.

(45) Papior, N.; Lorente, N.; Frederiksen, T.; García, A.; Brandbyge, M. Improvements on Non-Equilibrium and Transport Green Function Techniques: The next-Generation Transiesta. *Comput. Phys. Commun.* **2017**, *212*, 8–24.

(46) Brandbyge, M.; Mozos, J.-L.; Ordejón, P.; Taylor, J.; Stokbro, K. Density-Functional Method for Nonequilibrium Electron Transport. *Phys. Rev. B* **2002**, *65* (16), 165401.

(47) Datta, S. Nanoscale Device Modeling: The Green's Function Method. *Superlattices Microstruct.* **2000**, *28* (4), 253–278.

(48) Saha, K. K.; Nikolić, B. K.; Meunier, V.; Lu, W.; Bernholc, J. Quantum-Interference-Controlled Three-Terminal Molecular Transistors Based on a Single Ring-Shaped Molecule Connected to Graphene Nanoribbon Electrodes. *Phys. Rev. Lett.* **2010**, *105*

(23), 236803.

(49) Aprojanz, J.; Power, S. R.; Bampoulis, P.; Roche, S.; Jauho, A. P.; Zandvliet, H. J. W.; Zakharov, A. A.; Tegenkamp, C. Ballistic Tracks in Graphene Nanoribbons. *Nat. Commun.* **2018**, *9* (1), 1–6.

(50) Xie, H.; Kwok, Y.; Jiang, F.; Zheng, X.; Chen, G. Complex Absorbing Potential Based Lorentzian Fitting Scheme and Time Dependent Quantum Transport. *J. Chem. Phys.* **2014**, *141* (16), 164122.

(51) Calogero, G.; Papior, N. R.; Bøggild, P.; Brandbyge, M. Large-Scale Tight-Binding Simulations of Quantum Transport in Ballistic Graphene. *J. Phys. Condens. Matter* **2018**, *30* (36), 364001.